M. (1987) *Nature (London) 330*, 132–137.
Milne, R. W., Théolis, R., Jr., Verdery, R. B., & Marcel, Y. L. (1983) *Arteriosclerosis (Dallas) 3*, 23–30.
Mondola, P., & Reichl, D. (1982) *Biochem. J. 280*, 393–398.
Seman, L. J., & Breckenridge, W. C. (1986) *Biochem. Cell Biol. 64*, 999–1009.
Teng, B., Thompson, G. R., Sniderman, A. D., Forte, T. M., Krauss, R. M., & Kwiterovich, P. O., Jr. (1983) *Proc. Natl. Acad. Sci. U.S.A.* 80, 6662–6666.
Teng, B., Sniderman, A., Kwiterovich, P. O., Milne, R. W., & Marcel, Y. L. (1985) *J. Biol. Chem. 260*, 5067–5072.
Tikkanen, M. J., Cole, T. G., & Schonfield, G. (1983) *J. Lipid Res. 24*, 1494–1499.
Towbin, H., Staehlin, T., & Gordon, J. (1979) *Proc. Natl. Acad. Sci. U.S.A. 76*, 4350–4354.
Utermann, G., & Weber, W. (1982) *FEBS Lett. 154*, 357–361.
Utermann, G., Menzel, H. Y., Kraft, H. G., Duba, H. C., Kemmler, H. G., & Seitz, C. (1987) *J. Clin. Invest. 80*, 458–465.

Time-Resolved Solution X-ray Scattering of Tobacco Mosaic Virus Coat Protein: Kinetics and Structure of Intermediates†

M. Potschka,‡,§ M. H. J. Koch,∥ M. L. Adams,‡ and T. M. Schuster*,‡

Department of Molecular and Cell Biology, University of Connecticut, Storrs, Connecticut 06268, Max Planck Institute for Biophysical Chemistry, D-3400 Goettingen, FRG, and EMBL Outstation c/o DESY, Notkestrasse 85, D-2000 Hamburg, FRG

Received March 9, 1988; Revised Manuscript Received June 29, 1988

ABSTRACT: The kinetics of assembly and disassembly of tobacco mosaic virus coat protein (TMVP) following temperature jumps have been studied by small-angle X-ray scattering and turbidimetry. The structures of the principal aggregates of TMVP oligomers (A protein), intermediate size (helix I) and large size helical rods (helix II), have been characterized by their average radii of gyration of thickness, cross section, and shape obtained from the corresponding regimes of the small-angle scattering pattern. This structural information was obtained within seconds after the temperature-induced initiation of either polymerization or depolymerization and allowed us to detect transient intermediates. This methodology made it possible to observe and characterize the structure of a principal intermediate. Taken together with other kinetic information, these data suggest that polymerization of TMVP under virus self-assembly conditions may proceed via a single-layered helical nucleus that contains about 20 subunits. Previous studies have shown that overshoot polymerization of TMVP can occur and results in metastable long helical viruslike rods which subsequently depolymerize and then form short helical rods, depending on the conditions of the final equilibrium state. The longer rods (helix II) are overshoot polymers which form within seconds and contain $17^1/_3$ subunits per turn (helix IIB), in contrast to the subunit packing arrangement of $16^1/_3$ subunits per turn found in the shorter helical rods (helix IA). The latter packing arrangement is the one found in TMV. An overall polymerization scheme is proposed for the formation of these two helical forms of TMVP.

The assembly of tobacco mosaic virus (TMV)[1] has attracted continued interest for more than 30 years. One remarkable aspect of the properties of the components of this nucleoprotein complex is the fact that the coat protein, TMVP, alone can be made to self-assemble into viruslike rods. Although the assembly of TMV and of TMVP has been extensively studied, resulting in abundant data, and some models have been proposed, many central aspects of the assembly of the virus and of the coat protein remain unclear. As background, we provide only a brief summary of the more recent advances. Comprehensive accounts of the general subject have been given by Caspar (1963), Hirth and Richards (1981), Butler (1984), Stubbs (1984), Bloomer and Butler (1986), and Okada (1986) and in previous reviews cited therein.

Since TMVP can form viruslike rods in the absence of RNA, it is believed that many of the protein interactions in the virus are preserved in RNA-free helical structures. Depending on pH, temperature, protein concentration, and ionic strength, four major types of protein assemblies have been observed in solution: namely, at 100 mM ionic strength, oligomers (A protein), intermediate size polymers, and large helical polymers; at >0.4 M ionic strength, stacked disks (Klug & Durham, 1972). The structure of the long RNA-free helices has been studied by static fiber X-ray diffraction (Mandelkow et al., 1981). It was found that the helical RNA-free protein rods exist in two forms, one of which is the same as the native virus having $16^1/_3$ subunits per turn. The other is a polymorphic variant and has $17^1/_3$ subunits per helical turn. However, it was not known exactly which conditions of polymerization gave rise to each packing arrangement since all diffraction specimens were apparently prepared in the same manner. Originally, it was believed that all the long rodlike helical polymers found in weakly acidic conditions were structurally related to the virus (Holmes et al., 1975; Stubbs et al., 1977) and that the intermediate sized polymers in solution at pH 7, 20 °C, 100 mM ionic strength (20S polymers)

†This research has been supported by a grant from the National Institutes of Health (AI 11573) to T.M.S.
‡University of Connecticut.
§Max Planck Institute for Biophysical Chemistry
∥EMBL Outstation c/o DESY.

[1] Abbreviations: TMV, tobacco mosaic virus; TMVP, tobacco mosaic virus coat protein; SAXS, small-angle X-ray scattering; R_{G3}, R_{G2}, and R_{G1}, radius of gyration of shape, cross section, and thickness, respectively.

0006-2960/88/0427-8481$01.50/0

were bilayer disks,[2] a structure that has been crystallized from high ionic strength solutions and determined to 0.28-nm resolution (Bloomer et al., 1978). Two different pathways of assembly were believed to be responsible for these different polymer structures (Lauffer et al., 1967; Durham & Klug, 1972), and their modes of aggregation have been studied extensively (Lauffer, 1975; Butler & Durham, 1977; Schuster et al., 1980). Caspar (1963) proposed a unified model of sequential stepwise aggregation of subassemblies and provided arguments for an even more intricate model for these two different modes of assembly (Vogel et al., 1979). By acidifying intermediate sized polymer preparations, stacks of so-called lockwashers (short rodlike helical polymers) could be produced, and these slowly anneal to regular long helical polymers (Klug & Durham, 1972). Rather than being present in the initial solution, these short helical polymers were presumed to rapidly form from the bilayer disks by direct switching of the subunit packing arrangement, since it was believed that bilayer disks were the principal if not the only polymer species present at pH 7.0 and 100 mM ionic strength, i.e., virus assembly conditions (Butler & Durham, 1977). The presumed bilayer disk structure and its rapid kinetics of conversion to helices have never been verified in solution, however. Durham and Finch (1972) concluded that the majority of electron micrograph images were consistent with the bilayer disk aggregate but cautioned about possible staining, dilution, and surface artifacts. Recently, additional microscopic evidence for the existence of bilayer disks has been claimed by Turner et al. (1986). However, new experiments designed to test for the existence, in solution, of the bilayer disk have shown that it does not participate in either the nucleation or the elonation phase of virus assembly (Raghavendra et al., 1988a,b).

A refined picture of the TMVP assembly mechanism started to emerge along the above lines once the importance of kinetic effects was recognized (Scheele & Schuster, 1975). Intermediate size polymers were shown to elongate rapidly to large helices by addition of oligomers without lattice defects (Schuster et al., 1979). Elaborating earlier observations of Durham (1972) made it possible to demonstrate that intermediate size polymers are of variable length but larger than the size of the proposed 34-subunit bilayer disk (Schuster et al., 1980; Correia et al., 1985). Shire et al. (1979) characterized a polymerization nucleus containing about 35 subunits, but its relationship to the larger intermediate sized polymers was still speculative. Relaxation kinetic evidence that intermediate size polymers contain few if any bilayer disks (Potschka, 1983; Potschka and Schuster, unpublished results) is in agreement with the result of Raghavendra et al. (1985a), who found that polymers formed at high ionic strength under bilayer disk crystallization conditions are spectroscopically different from those at 100 mM ionic strength. Because of their similar yet different nature, the two types of polymers observed at 100 mM ionic strength have been named helix I (formerly called intermediate sized polymers) and helix II (formerly called large helical polymers) (Potschka & Schuster, 1987). At 100 mM ionic strength, TMVP assembly has been shown to follow a nucleation controlled mechanism of overshoot polymerization (Scheele & Schuster, 1975) even at the standard conditions for viral assemblies studies (pH 7, 20 °C) (Potschka and Schuster, unpublished results).

These findings appear to be in agreement with a recent report by Namba and Stubbs (1986) that questions the original model proposed for the process of protein–RNA recognition and the reconstitution of virions (Butler & Klug, 1971; Klug, 1983). We have studied TMVP nucleation and polymorphism in more kinetic and structural detail using time-resolved X-ray solution scattering in order to further clarify the protein–protein interactions in TMVP. We present evidence that (1) the principal nucleation intermediate may be a single-layered structure and not bilayer disks or three-layered sheets and (2) overshoot polymers rapidly formed by oligomers contain $17^1/_3$ subunits per turn. (3) We summarize evidence that polymerization at 100 mM ionic strength can be described by a single reaction scheme which entails nucleation and elongation for both helical forms.

Materials and Methods

Sample Preparation. TMV (common strain) was isolated from infected tobacco leaves (kindly supplied by Dr. C. A. Knight) and purified by the method of Paglini and Lauffer (1968) as modified by Shire et al. (1979). TMVP, prepared by the modified acetic acid degradation method of Scheele and Lauffer (1967), was dialyzed against the appropriate buffer for 48 h and stored at 0 °C for at most 2 weeks. All TMVP experiments reported here were made in phosphate buffers of 100 mM ionic strength; the samples used for X-ray scattering also contained 1 mM NaN_3, but those samples used for obtaining the other data reported did not. The addition of 1 mM NaN_3 does not affect protein aggregation (Schuster et al., 1979). Special precautions were taken to avoid plant proteases and bacterial contamination (Steckert, 1982). Protein concentrations were determined spectrophotometrically (ϵ_{282} = 1.20 mg^{-1} cm^2) and verified by their relative scattering intensities in their oligomeric aggregation state.

Optical Kinetic Measurements. A solenoid valve switching device between two water baths was used to perform slow temperature jumps (with a heating time $\tau \sim 50$ s) with conventional jacketed quartz cuvettes. The time course of turbidity was monitored in a Varian Cary 118C spectrophotometer at 313 or 291 nm. The latter is an isosbestic point in the aggregation-related changes of optical absorbance (Schuster et al., 1980). Light-scattering changes at 90° were also followed by using a modified Brice–Phoenix 2000 photometer.

Small-Angle X-ray Scattering Experiments. X-ray solution scattering experiments were carried out at the EMBL Outstation of the DORIS-I storage ring of the Deutsches Elektronen Synchrotron (DESY) in Hamburg.

Measurements were taken on the double-focusing mirror monochromator cameras X13 (Hendrix et al., 1979) and X33 (Koch & Bordas, 1983) in HASYLAB and recorded using a linear position sensitive detector with delay line readout and a flow of a 80:20 mixture of Ar/CO_2 (Gabriel, 1977). With a sample to detector distance of 1–3.5 m, the total range of scattering vectors was $0.013 < s\ (nm^{-1}) < 0.4$ ($s = 2 \sin \theta/\lambda$, were 2Θ is the scattering angle and the wavelength $\lambda = 0.15$ nm). Drifts of the beam position of DORIS caused excessively large scatter of data for $s < 0.02$ nm^{-1}. Time-resolved scattering patterns were collected during temperature jumps (Bordas et al., 1980) in sequences of 250 frames of 3- or 60-s duration each. Static data were accumulated for 60–30 s. Samples were kept in a 200-μL temperature-controlled scattering cell with mica windows, equipped with four thermostat baths and a rapid switching device (with a heating time $\tau \sim 4.6$ s) (Renner et al., 1983).

[2] We use the term TMVP "bilayer disks" to refer to the 2-layer, 17 subunit per layer, cylindrical structure identified in crystals of TMVP grown from high ionic strength buffers (Bloomer et al., 1978). We, and others, have previously referred to this structure as "disks" or "double disks" (Lauffer, 1975), but this nomenclature becomes ambiguous when discussing one-layer structures as well as two-layer structures and their aggregates.

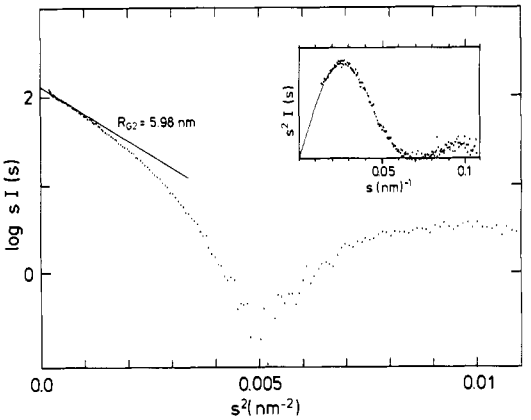

FIGURE 1: Cross-sectional small-angle scattering of TMV. Points represent individual detector channels, accumulated for 300 s at a virus concentration of 3 mg/mL, and are not desmeared. The first maximum of the insert corresponds to $2\pi sR_G = 1$ which limits the Guinier region of R_{G2}.

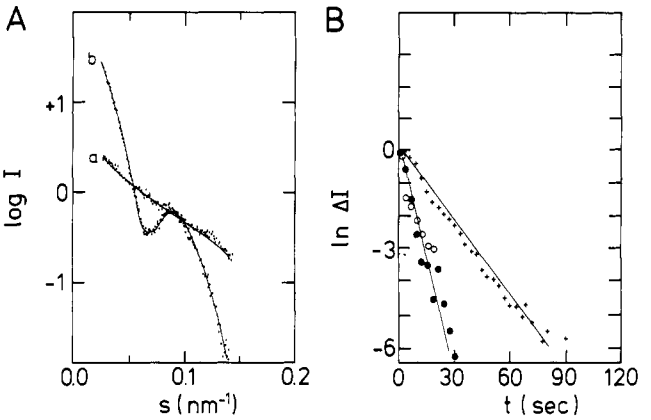

FIGURE 2: TMVP overshoot polymer formation. SAXS of oligomers and large helix II overshoot polymers (A) and rate of polymerization followed by the integral scattering in the range $0.02 < s$ (nm^{-}) < 0.04 and normalized to unit reaction amplitudes (B). 22 mg/mL TMVP, pH 6.5, kept on ice for several days to dissociate all polymerization nuclei, was injected into a thermostated cell, that was previously equilibrated at 5 °C, and measured in its oligomeric form within 10 min (A, curve a). The temperature was then raised to 20 °C with a heating rate of $\tau = 4.6$ s [B (○)]. The formation of long helix II polymers proceeded within the time of heating [B (●)] and was complete after 30 s. The full SAXS spectrum was measured every 3 s; shown is the trace averaged from 60 to 120 s (A, curve b). Ten minutes later, the polymers were dissociated by returning to 5 °C. They decayed with a single first-order rate $\tau = 13.5$ s [B (+)] to a state whose SAXS was almost indistinguishable from the initial oligomeric one (A, curve a).

Each region of the scattering envelope (Guinier & Fournet, 1955) is independent of the next largest dimension of a particle for $s^{-1} > 2\sigma R_G$ (Mittelbach, 1964). For R_{G2}, the latter corresponds to a maximum in a s^2I vs s plot (Kratky, 1982). Upward deviations from the extrapolation through the origin indicate aggregation, downward deviations occur if the largest dimension of the particle becomes similar to the quadratic average of the other two dimensions. The latter statement is more clearly seen in a log sI vs s^2 plot. Additional information can be retrieved from the position of the minima and maxima and their relative intensities.

RESULTS

Small-Angle X-ray Scattering of TMV. Figure 1 illustrates the scattering pattern of TMV. Note the sharp minimum obtained without desmearing. The position of the maximum in the insert of Figure 1 determines the appropriate regime of the two-dimensional Guinier plot used to obtain R_{G2}. This yields a value of $R_{G2} = 6.0$ nm. The innermost data points deviate upward, indicating the occurrence of a few percent of lateral virus aggregates. Since the R_{G2} value of lateral dimers is at least 1.6 times larger than those of single virus particles, they introduce little error in the calculation of virus cross section. Only axial aggregates of the virus have been characterized previously in detail (Steere, 1953), but the occurrence of tactoid gels of TMV in plant cells [reviewed by Esau (1968)] and in solution (Bernal & Fankuchen, 1941) suggests that lateral aggregates exist in solution as well. The intensity of the first side maximum relative to $(sI)_0$ (Mittelbach, 1964) corresponds to a hollow cylinder with $r_{in} = 1.5$ (±0.5) nm and $r_{out} = 8.4$ (±0.5) nm. These values are to be compared with the corresponding values of 1.5 and 9.0 nm as determined by Caspar (1956) and Franklin (1956).

Structure and Kinetics of Long Helical Rods (Helix II). The formation and dissociation of overshoot helix II polymers are illustrated in Figure 2. A pure oligomer sample at pH 6.5 was rapidly warmed, and the time course of the formation and elongation of polymers was monitored. Then the sample was cooled again to follow the time course of dissociation. The turbidity amplitude during successive heating cycles is always smaller than that in the previous cycle (Schuster et al., 1979) which proves that nuclei are formed within the first seconds of the initial temperature perturbation and are retained while new nuclei form. In separate experiments, we determined the rate of nuclei dissociation at pH 6.5 and 2 °C ($k_{off} = 3 \times 10^{-4}$ s^{-1}) and at 0.3 °C ($k_{off} = 1 \times 10^{-3}$ s^{-1}) (turbidity data not shown). Data for 6.5 °C ($k_{off} = 7 \times 10^{-7}$ s^{-1}) have been reported by Shire et al. (1979).

Since the diameter of the TMVP helical rods is uniform, the monitored SAXS signal is proportional to the number of subunits incorporated. This is an advantage over nonlinear orbital turbidity amplitudes that are commonly employed and permits a reliable assessment of the rate of stepwise dissociation of oligomers ($k_{off} = 7 \times 10^{-2}$ s^{-1}) (Figure 2B). Given an association time of less than 4 s (Figure 2B) and some 10^3 sequential elongation steps (estimated from the size of these polymers according to sedimentation coefficients and electron micrographs), the intrinsic association rate constant must be at least of the order of $k_{on} = 1 \times 10^6$ s^{-1} M^{-1} (estimated as 4 ms per trimer at approximately 0.3 mM TMVP trimer concentration). Within the errors of measurement (i.e., ±15%

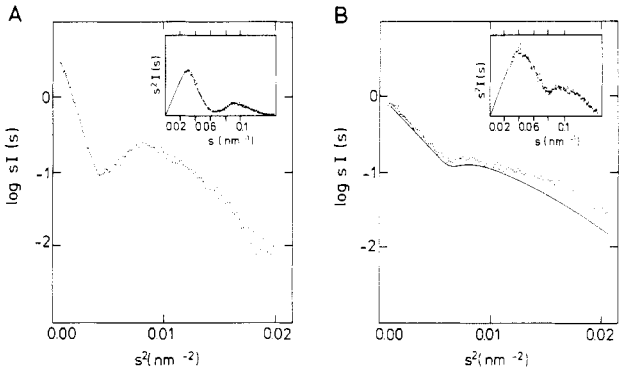

FIGURE 3: Cross-sectional representation of the small-angle scattering of TMVP polymers. (A) Helix II type polymers (>200 nm long having a sedimentation coefficient $s_{20,w} > 150$ S) obtained by overshoot polymerization at 20 °C of 22 mg/mL TMVP, pH 6.5 (Figure 2). There are not enough data points to define the two-dimensional Guinier region reliably (insert), but from $s_{1min} = 0.068$ nm^{-1} and $s_{1max} = 0.089$ nm^{-1}, the radius of gyration $R_{G2} = 6.5$ (±0.1) nm can be calculated. (B) Helix I type polymers (about 5–7 nm long having an intrinsic sedimentation coefficient $s^0_{20,w} = 20.4$ S): 13 mg/mL TMVP, pH 7.0, 20 °C, at equilibrium containing 80% polymers and 20% oligomers (•). The pure polymer scattering pattern (—) is obtained by subtracting the oligomer contribution. $S_{1min} = 0.079$ nm^{-1}; $R_{G2} = 4.2$ nm is estimated from the Guinier region as defined by the insert.

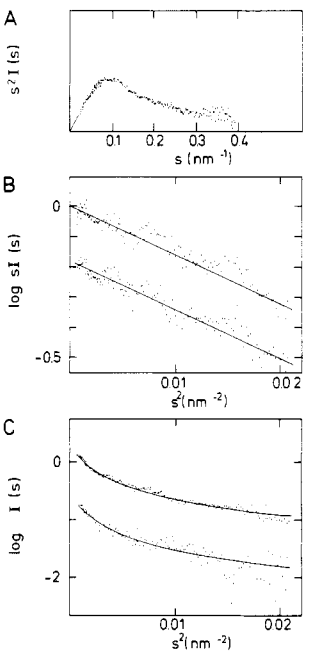

FIGURE 4: Small-angle scattering of TMVP oligomers using three types of data representation. (A) 13 mg/mL TMVP, pH 7.0 at 5 °C. The Guinier scattering region of the cross section extends to $s < 0.14$ nm^{-1}. No side maxima are observed. (B) 22 mg/mL TMVP, pH 6.5 at 5 °C, slope $R_{G2} = 1.48$ nm (upper curve); and 13 mg/mL TMVP, pH 7.0 at 5 °C, slope $R_{G2} = 1.50$ nm (lower curve). (C) 13 mg/mL TMVP, pH 7.0 at 5 °C (upper curve), and 3 mg/mL TMVP, pH 7.0 at 5 °C (lower curve). For a discussion of R_{G3}, see the text.

in amplitude), the rates of formation and dissociation of overshoot polymers do not depend on the scattering vector choosen for analysis (data not shown).

Compared with the scattering pattern of the virus (Figure 1), the SAXS pattern of these TMVP helix II rods (Figure 3A) shifts to smaller angles, and $R_{G2} = 6.5$ (±0.1) nm can be derived only from the position of the first minimum and maximum (Mittelbach, 1964). The relative intensity of the first side maximum increases and corresponds to a hollow cylinder with $r_{in} = 2.3$ (±0.5) nm and $r_{out} = 8.9$ (±0.5) nm. The expected radii of gyration are easily computed from the radial density distributions obtained by fiber diffraction (Mandelkow et al., 1976) and are $R_{G2} = 6.0$ nm for the virus, $R_{G2} = 6.1$ nm for the RNA-free helix which like the virus contains $16^1/_3$ subunits per turn, and $R_{G2} = 6.5$ nm for the RNA-free helix having $17^1/_3$ subunits per turn. Mandelkow et al. (1976) distinguish between these two subunit packing arrangements by designating $16^1/_3$ as helix A and $17^1/_3$ as helix B. Our long overshoot helix II rodlike polymers thus are type B helices. Previous electron microscopic studies had shown that the overshoot polymers are long helical rods but on the basis of this gross morphology alone the subunit packing could not be distinguished from that in the virus (Schuster et al., 1979).

Structure of Short Helical Rods (Helix I). The scattering of helix I shown in Figure 3B is quite distinct from that of helix II (Figure 3A). The value of $R_{G2} = 4.2$ (±0.1) nm (five determinations) for helix I is consistent with the position of the maximum in the s^2/I vs s plot. The ratio $s_{1max}/S_{1min} < 1.3$ indicates that the two minor axes are not equal (Mittelbach, 1964). Both features are consistent with the known average molecular weight (Correia et al., 1985) which corresponds to cylinders less high (~5–7 nm) than wide (18.0 nm). For oblate shapes, it is meaningful to determine an apparent thickness from the slope of a log s^2/I vs s^2 plot. Here the one-dimensional Guinier regime extends from $2\pi sR_{G2} > 1$ to $2\pi sR_{G1} = 1$ but is frequently rippled so that interpolation of the oscillations measured out to larger angles proves to be more reliable and prevents overestimates of R_{G1} that could arise from a superimposed peak at $2\pi sR_{G2} = 1$ (Mittelbach, 1964). At pH 7.0, 20 °C, and polymerization equilibrium conditions, we obtain $R_{G1} = 1.8$ (±0.2) nm. As a first approximation, this result corresponds to a thickness of 7 nm for an elliptic cylinder (Mittelbach, 1964). Given the helical topology and the fact that the maximum thickness dominates the radius of gyration, the actual weight-average degree of polymerization corresponds to a few subunits less than three helical turns. The upper limit for the expected value of R_{G2} is the maximum dimension of the cross section which is a rectangle 7 by 17 nm and yields a calculated value of $R_{G2} \sim 4.5$ nm. Due to the small difference between R_{G3} and R_{G2} for helix I particles, the two-dimensional Guinier regime is ill-defined, but the self-consistency of our data for R_{G2} measured and estimated from R_{G1} is satisfying. With only 10 channels of data available when $s < 0.024$ nm^{-1}, no useful R_{G3} may be computed. Presently, it is not possible to decide by SAXS data alone whether helix I polymers contain $16^1/_3$ or $17^1/_3$ subunits per turn. However, we do know from extensive studies under these conditions (Shire et al., 1981) that these short helical rods, which have an intrinsic sedimentation coefficient $s^0_{20,w} = 20.4$ S, are capable of nucleating the virus reconstitution reaction. So we presume that they have the $16^1/_3$ packing arrangement. This does not rule out the possibility that nonequilibrium conditions for short helical rods may yield $17^1/_3$ packing arrangements.

Small-Angle X-ray Scattering of Oligomeric TMVP (A Protein). The scattering of the 4–6S A protein, which predominantly contains trimers, is featureless (Figure 4). At 5 °C, the shape of the scattering envelope is virtually independent of protein concentration (up to at least 22 mg/mL) or pH [up to at least pH 12 (Anderer et al., 1964)]. The two-dimensional Guinier region is surprisingly well-defined and yields $R_{G2} = 1.5$ nm (Figure 4B), in agreement with the position of the maximum in Figure 4A. This slope cannot originate from a triangular- or wedge-shaped trimer since its largest dimension would be approximately 7 nm and we would

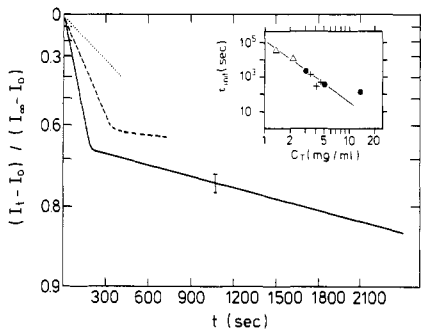

FIGURE 5: Semilogarithmic plot of the rate of helix I formation at pH 7.0, 20 °C, monitored by integral scattered intensity in the range $0.02 < s\ (nm^{-1}) < 0.04$. Protein concentrations are 13 mg/mL (—), 5 mg/mL (---), and 3 mg/mL (···). The scatter of individual data points (not shown) corresponds to the scatter of data in Figure 7 and is indicated by error bars. An even more rapid process occurss within the heating time. It has at most 1% of the total reaction amplitude and is not apparent on this scale. Insert: Double-logarithmic plot of the initial rates as a function of protein concentration, monitored by the integral SAXS intensity as above (●), by scattered light intensity at 90° (+), and by turbidity at 291 nm (△).

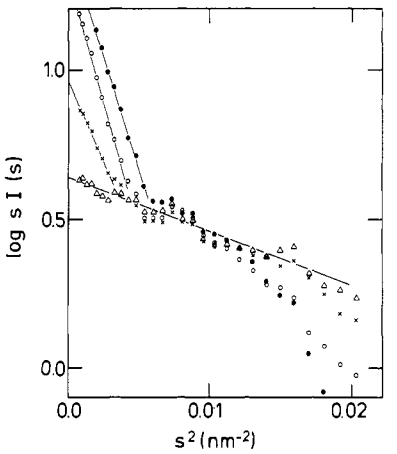

FIGURE 6: Scattering properties during formation of helix I polymers at pH 7.0, 20 °C, 13 mg/mL TMVP. Scattering profile at 5 °C just before temperature jump to 20 °C (△), during the first 60 s after reaching 20 °C (×), after 300 s at 20 °C (○), and at equilibrium (at least 24 h at 20 °C) (●). Each point corresponds to the added intensity of five consecutive data channels. The average time dependency of the signal at small angles [$0.02 < s\ (nm^{-1}) < 0.04$] is shown in Figure 5.

expect to observe a pronounced downward curvature of the data at low angles (Mittelbach, 1964). This inconsistency is corroborated by the slope of log I vs s^2 (Figure 4C) for $0.03 < s\ (nm^{-1}) < 0.04$ which gives an apparent $R_{G3} = 5.4$ nm (for which the appropriate region of measurement actually is $s < 0.03\ nm^{-1}$). This is much larger than is possible for trimers since all reasonable estimates for conceivable shapes of native TMVP trimers (Caspar, 1963) result in values of $R_{G3} < 4$ nm. In addition, the method of obtaining the maximum particle dimension by combination of R_{G2} and R_{G3} (Anderer et al., 1964) yields a value of 16 nm which is also inconsistent with a simple native trimer model.

The SAXS data thus unambiguously confirm the presence of oligomers larger than trimers, possibly as large as heptamers (Kazel, 1981), that contribute differently at different s vectors. Since A protein also contains some monomer one ought to be cautious in interpreting the apparent slope of $R_{G1} \sim 0.5$ nm [see Figure 8 (△)]. However, all the A protein data in Figure 4 demonstrate that very similar distributions of oligomers exist at the variety of conditions studied.

Rate of Formation of Short Helical Rods (Helix I). The formation of helix I polymers at pH 7, 20 °C, from pure oligomer samples is shown in Figure 5. The reaction is biphasic; however, turbidity experiments have revealed a final third phase (Schuster et al., 1980) not recorded during the shorter duration X-ray scattering experiments. The initial rates observed by X-ray scattering intensities agree with conventional optical measurements using turbidity or light scattering (Figure 5 insert) and are markedly concentration dependent. From the slope of a double-logarithmic plot of these data, we obtain an apparent kinetic order of the nucleation reaction, $n = 3.5$ (±0.5). The deviations at high concentrations are expected, since we plot total protein mass, not moles, and $M_w/M_n > 1$ and is known to increase with concentration (Kazel, 1981). These observed initial rates agree with the rates of final approach to equilibrium, where the concentration of trimers is decreased to about 1 mg/mL at pH 7.0, 20 °C (Schuster et al., 1980). Within experimental error, the initial rates are independent of scattering angle in the range of $0.02 < s\ (nm^{-1}) < 0.04$ (data not shown).

However, the definite biphasic nature of the reaction is not consistent with the simple disappearance of oligomers. A closer examination of the SAXS pattern corroborates this view (Figure 6). Within the first 60 s of reaction, the polymers approach their final R_{G2} values. This means that there is rapid attainment of the final cross-sectional shape. However, since only few polymers exist after 60 s, the average scattering intensity for $s > 0.1\ nm^{-1}$ remains dominated by oligomers. The initial rate of polymerization monitored in the region $0.1 < s\ (nm^{-1}) < 0.14$ is identical with the corresponding concentration in Figure 5 (data not shown). At the end of the initial phase (200 s), full-size helix I polymers exist [Figure 6 (○)], and the scattering intensity for $s > 0.1\ nm^{-1}$ changes little at later times. The amount of helix I, however, continues to increase with a slight decrease of R_{G2}. These data confirm sedimentation studies that show the absence of helix II polymers at pH 7.0 and 20 °C in 100 mM phosphate, i.e., commonly used conditions for virus reconstitution experiments. Previous turbidity and sedimentation studies have shown that the overshoot polymerization reaction of TMVP is extremely pH dependent (Scheele & Schuster, 1975; Schuster et al., 1979). Although those methods did not reveal overshoot polymerization at pH values above 6.7 because of the small amplitudes and rapid decay times to equilibrium, the initial slopes of the scattering envelopes in Figure 6 suggest that helix I polymers at pH 7.0 may also pass through a transient maximum, possibly confined to helix I polymers.

Light-scattering experiments (data not shown), performed at the same pH 7.0, 20 °C, gave the following results: at 10 mg/mL, a clearly observable transient turbidity maximum[3] with $\Theta_{max} = 0.08$ (±0.01) was observed; the final approach to equilibrium was $\tau \lesssim 1 \times 10^5$ s. At 22 mg/mL, we again observed $\Theta_{max} = 0.08$ (±0.01). No turbidity maximum was found at 5 mg/mL, 20 °C. Since $d\Theta_{max}/dc_T > 0$ for an infinite polymerization (Scheele & Schuster, 1974), these data demonstrate that the size to which helix I polymers may grow is limited since they become unstable beyond a certain size. These findings indicate that the small observed overshoot at pH 7.0 is mostly a transient increase of size within the distribution of helix I polymers and not the formation of helix II polymers.

Dissociation of Short Helical Polymer Rods (Helix I). The rate of helix I dissociation (Figure 7) is nearly independent

[3] $\Theta_{max} = (\langle i \rangle_{max} - \langle i \rangle_{equil})/\langle i \rangle_{equil}$ where $\langle i \rangle$ is the average degree of polymerization. For derivation and explanation of this key relationship, see Scheele and Schuster (1974).

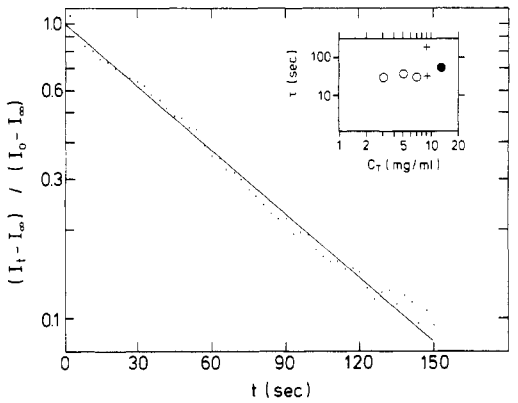

FIGURE 7: Semilogarithmic plot of the rate of helix I dissociation starting with polymerized samples at pH 7.0, 20 °C. 13 mg/mL TMVP, final temperature 5 °C. The decay is monitored by the integral scattering intensity in the range $0.02 < s$ (nm^{-1}) < 0.04. Insert: Double-logarithmic plot of the rate of dissociation as a function of total protein concentration at final temperatures of 4 °C (○), 5 °C (●), and 6.5 °C (+). The biphasic decay at 6.5 °C is analyzed in more detail in Figure 8. Note the extreme temperature dependence.

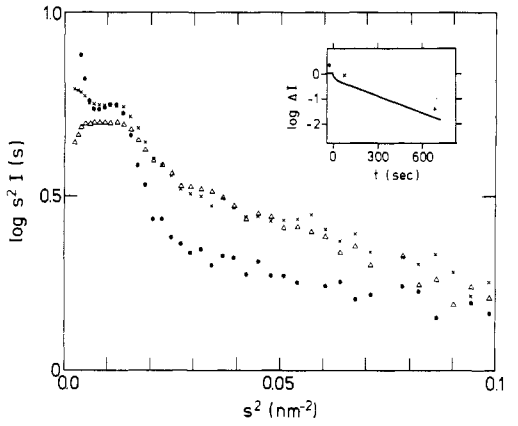

FIGURE 8: Transient measurement of intermediate aggregate upon polymer dissociation at pH 7.0, 6.5 °C. 9 mg/mL TMVP at pH 7.0, 20 °C, and containing 80% polymers (●) was measured 40–70 s after initiation of dissociation by lowering the temperature to 6.5 °C (×) and again after 650–680 s (△). Each plotted point corresponds to the added intensity of three consecutive data channels. Insert: Progress of dissociation monitored by integral intensity in the range $0.02 < s$ (nm^{-1}) < 0.04. The time points at which full SAXS spectra are shown are indicated with their respective symbols. The values for the two relaxation times obtained are included in the insert of Figure 7. At $t = 0$, the temperature decreases from 20 °C to 6.5 °C.

of polymer concentration. At pH 7.0 and 6.5 °C, dissociation is biphasic (Figure 8 and Figure 7 inserts). Closer inspection of the transient structures reflected in the scattering envelopes in Figure 8 reveals that the fast phase corresponds to stepwise dissociation of subunits down to the size and thickness of some polymer nucleus and the slow phase corresponds to its dissociation. In order to analyze the transient scattering patterns in these depolymerization experiments, we have calculated simulated scattering profiles of mode shapes (Figure 9). In the one-dimensional Guinier region, $s > 0.1$ nm^{-1}, the intermediate polymers themselves contribute to the observed slope of $R_{G1} \sim 0.5$ nm. On the basis of a mass balance calculation and the simulations, the size of the 6.5 °C transient intermediate is about half the thickness and mass of the 20S polymer at 20 °C. Other measurements have shown this 20S structure to be composed of 39 subunits, each of M_r 17 530 (Correia et al., 1985).

In separate experiments, we have estimated this nucleus size by the decrease of turibdity upon depolymerization of helix I preparations of known size. At pH 6.5, 7 °C, we estimate

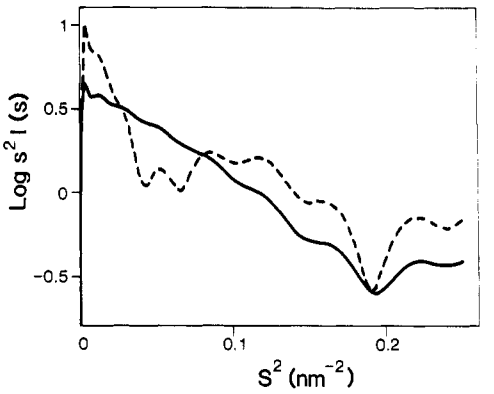

FIGURE 9: Simulated scattering patterns of a hollow cylinder of radius $r_{out} = 8.4$ nm and $r_{in} = 2.3$ nm and two heights (h) as follows: simulated single-layer disk ($h = 2.3$ nm) (—) and bilayer disk ($h = 4.6$ nm) (---). For the single disk, the one-dimensional Guinier region is well-determined and yields the correct slope R_{G1} with the formula for infinite plates that is used in the analysis of the experimental data. The region $0 < s^2$ (nm^{-2}) < 0.1 for the single-layer disk of this figure should be compared with Figure 8 (△).

an intermediate structure with 35 (±5) subunits; at 0.3 °C, one with 25 (±5) subunits. Similar values were observed at pH 7.0 at 16 and 10 °C, respectively. Upon returning the latter sample (10 °C) to 20 °C, polymerization was substantially faster compared with a sample that was first quenched at 0 °C to dissociate all nuclei. At lower temperatures at pH 7.0, the slow phase of dissociation became too fast for our two-water bath switching method to estimate the transient intermediate size by light scattering. It is, however, clear from these data that the size of the transient intermediate nucleus changes with the solution conditions (see Discussion).

The temperature dependence of helix I dissociation (Figure 7 insert) shows a pronounced temperature effect on the rate of nucleus dissociation and little if any effect on the prior stepwise removal of subunits ($k_{off} = 3 \times 10^{-2}$ s^{-1}). Below 4 °C, the rate-limiting reaction is the sequential removal of subunits, and therefore only a single kinetic phase is observed.

Discussion

Our application of time-resolved small-angle X-ray scattering to the study of the self-assembly of tobacco mosaic virus coat protein has revealed new information about the existence and structure of intermediates in both the polymerization and depolymerization reactions of the TMVP subunits. In addition, we have obtained kinetic data which further characterize the nucleation-controlled polymerization mechanism of TMVP. The identification of transient intermediate single-layer polymers leads us to suggest that these single-layer structures (partial helical arrays of subunits) may be the critical nuclei that rapidly elongate with oligomers to form larger helical rods of two size classes, helix I or helix II, each of which may exist in one of two subunit packing arrangements, helix A or helix B. These new data have lead us to reconsider the widely reported so-called "phase diagram" of TMVP assembly (Butler & Durham, 1977; Butler, 1984) and the kinetic mechanism for TMVP assembly and overshoot (Schuster et al., 1979). Figures 10 and 11 show a schematic assembly model which summarizes the known species involved in the assembly–diassembly of helical TMVP rods. In this section, we discuss briefly each class of polymer with special emphasis on the results obtained in the present study.

Virus and Helix II. The radius of gyration of the cross section of TMV (Figure 1) agrees well with the value of $R_{G2} = 5.9$ nm reported by Kratky et al. (1957) and with the radial

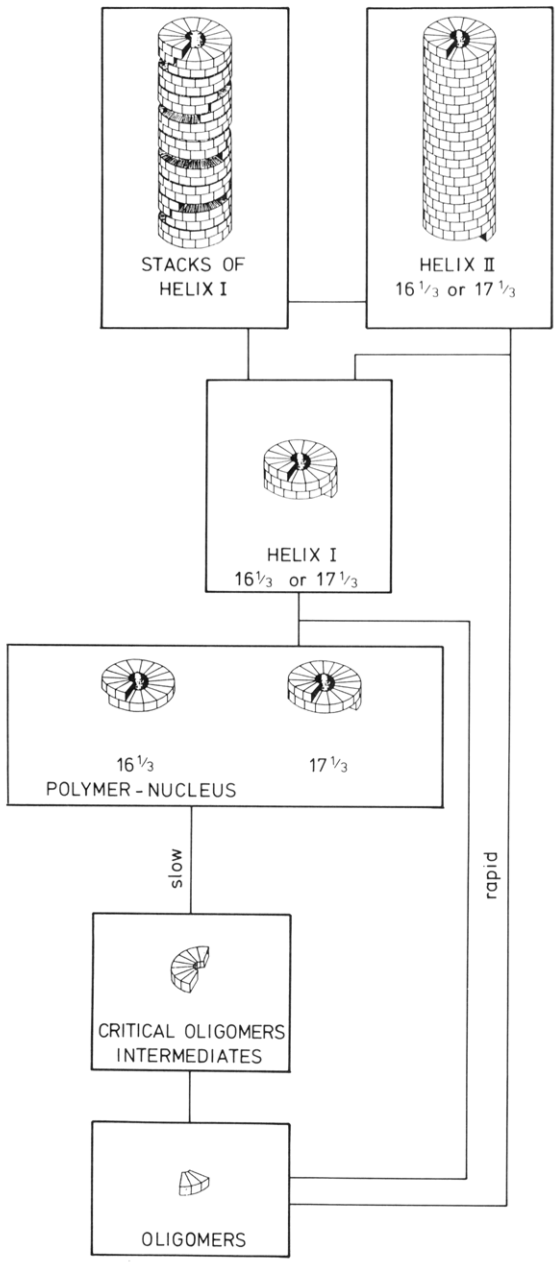

FIGURE 10: Schematic summary of the proposed pathway of assembly of TMVP. Oligomers of various sizes aggregate to form a nucleus that occurs in two polymorphic forms, each leading to different polymers. Helical nuclei may rapidly elongate to small helices having lengths of 1–4 turns with either $16^1/_3$ or $17^1/_3$ subunits per turn. Since elongation by oligomers is fast compared to nucleation, one observes characteristic kinetic patterns, termed overshoot polymerization. Helix I aggregates may either stack or add oligomers to yield a different conformation, helix II, that again occurs with $16^1/_3$ or $17^1/_3$ subunits per turn. Each class of aggregate and dynamic network is described under Discussion.

density distribution obtained by fiber diffraction (Mandelkow et al., 1976). Although the radial density inhomogeneities influence the pattern of side maxima (Fedorov, 1971), they have little influence on R_{G2}. Removal of the RNA increases R_{G2} slightly, but the effect is small compared with the change between the $16^1/_3$ subunits per turn packing in helix A and the polymorphic variant helix B with $17^1/_3$ subunits per turn. Since we also observe an increase in the relative intensity of the first side maximum, we are confident that the structure of the overshoot polymers corresponds to type B, and we will refer to those helical rods from now on as helix IIB.

The type A–type B polymorphism is not understood, but it is known that residues 90–113 in TMVP are disordered in

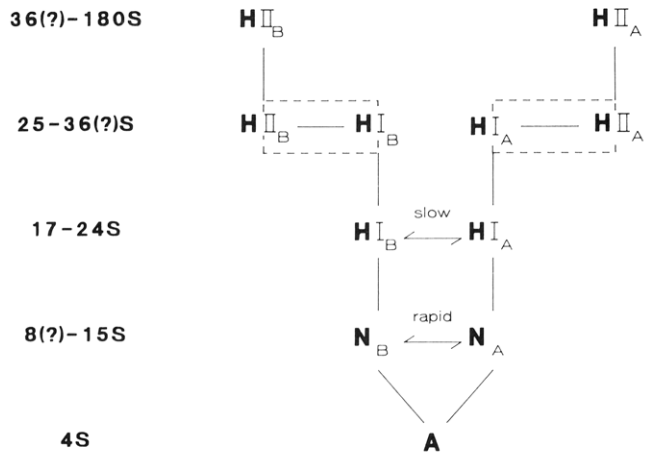

FIGURE 11: Detailed reaction scheme excluding any reactions that result from self-association of polymer species. A stands for oligomers (A protein), N for nucleus, H I for helix I, and H II for helix II. The corresponding size ranges are indicated as sedimentation coefficient values. Not shown is the coupling of this length-dependent subunit packing scheme with protonation which would add another dimension to the network graph. The figure highlights first the transition between helix I and helix II where we envisage a cooperative conformational change coupled to aggregate size such that both conformations coexist for the same size aggregates only over a limited size range. Second, the figure emphasizes the branching of the polymerization into two pathways, one with $16^1/_3$ subunits per turn (type A) and the other with $17^1/_3$ subunits per turn (type B). There may be a rapid interconversion of these states for polymers the size of nuclei (but still slower than oligomer addition represented by vertical steps). Interconversion must become very slow as aggregate size increases. An interconversion pathway via oligomers (4 S) may be a viable alternative to direct polymer (8–15 S) interconversion. Whether type A nuclei form via type B nuclei or via a polymorphic variant of A protein (not shown) is not known.

the cylindrical bilayer disk crystal formed at high ionic strength (Bloomer et al., 1978) whereas in the intact virus this chain region is ordered as a large loop region that sequesters the RNA from the inner hole in the virus (Namba & Stubbs, 1986). In RNA-free helix II, the region is in a similar but not identical conformation with that of the virus (Mandelkow et al., 1981). It is further known from NMR data that this region is flexible (disordered) in helix I but rigid (ordered) in helix II (Jardetzky et al., 1978). Furthermore, Mandelkow et al. (1981) claimed that the side chain of Arg-92 is more disordered in type B than in type A helices. While the structural differences between the bilayer disk and the helical virus possibly result from ionic strength effects, the differences between the type A and type B helix are probably the result of kinetic effects in which the very rapid rate of subunit addition to nuclei may trap transient type B nuclei which form faster than type A nuclei even though the latter may represent a more stable subunit packing arrangement. Detailed answers will have to wait for additional systematic investigations. Our data, however, disprove an older speculation that helix IIA forms by rapid polymerization of oligomers whereas helix IIB forms from the then-presumed disklike intermediate sized polymers [Caspar, 1976; however, see also Raghavendra et al. (1986)]. The only evidence for polymorphism at the oligomer level of subunit association concerns different states of protonation, but it is not known if oligomer protonation relates to structural polymorphism. For this reason, we have only drawn one A-protein species into Figure 11.

Helix I. The SAXS analysis of TMVP at pH 7.0 and 20 °C results in a characterization of helix I as short rods which are less high than they are wide. This model agrees with weight-average degree of polymerization data obtained by sedimentation equilibrium studies of TMVP prepared the same

way and at the same pH and temperature (Correia et al., 1985). These results and the kinetic patterns observed confirm that helix I polymers are larger on average than would be expected for a bilayer disk (34-mer). We have shown that the helix I polymer's average size varies with the conditions of equilibrium (pH and temperature) (Schuster et al., 1980; Potschka, 1983; Correia et al., 1985) as well as during the phases of their formation and dissociation. Judged by rapid relaxation kinetic experiments (Potschka and Schuster, unpublished results), helix I polymers occur in a unimodal distribution of various sizes, and we thus have reason to believe that their topology is that of an open subunit assembly like a helix rather than a closed structure like a cylinder. This view is in line with the earlier data on assembly by Klug and Durham (1972). The compounded evidence [see also Raghavendra et al. (1988a,b)] is however at variance with recent reports which insist on the bilayer disk nature of these polymers (Butler, 1984; Turner et al., 1986).

Helix I polymers can rapidly grow and interconvert to helix II polymers, and all experiments thus far are consistent with the notion that helix I is the precursor of helix II (Schuster et al., 1979; Potschka and Schuster, unpublished results). However, the detailed conformation of subunits in the helix I structure must be different from that in helix II as judged by the spectroscopic evidence (Jardetzky et al., 1978; Potschka, 1981, 1983; Raghavendra et al., 1985b) and the limited size of helix I [see also Potschka and Schuster (unpublished results)]. The similar aggregation properties of the two subunit structures and possible sources for the subtle structural difference between helix I and helix II have been discussed by Raghavendra et al. (1985b) and by Potschka and Schuster (1987). The polymorphism of type A and type B helices involves slippage between helical turns, and the rate of direct interconversion, if it occurs, is expected to decrease strongly with the number of subunits present in excess of minimal nucleus sizes. It is for this reason that we believe that the type of helix II packing may be determined by the transient precursor helix I packing.

Nucleation Intermediates. Most experimental evidence on nucleation intermediates relies on kinetic approaches since nucleus concentrations are too low to be detected by equilibrium techniques. However, kinetic experiments may be designed to yield information about nucleation intermediates in terms of both transient structures and kinetic parameters. Similar strategies have been employed in studies of tubulin (Bordas et al., 1983; Spann et al., 1987). We have gathered evidence concerning (1) the rate at which TMVP nuclei form, which yields information about the large oligomer precursor states, (2) the pattern and rate of polymer dissociation, which provide information on the stability of a transient nucleus, and (3) the structure and size of this nucleus deduced from time-resolved small-angle X-ray scattering.

(*1*) *Minimum Nucleus Size.* Formation of helix I polymers proceeds via nucleation followed by a limited extent of elongation polymerization. Since the consecutive addition of subunits is rapid, requiring no more than a few seconds in all (Potschka and Schuster, unpublished results), it is nucleation that determines the initial rate of helix I formation. The formation of nuclei is itself a complex process that involves the kinetic coupling of several sequential association steps. Provided that the concentrations of larger oligomers decrease continually with size, which appears to be the case (Kazel, 1981), the rate-limiting step will be the bimolecular recombination of two large oligomers of the same or similar size that yield a product at least as large as the nucleus. We shall refer to this process as a random dimerization, since the critical oligomer size is half that of the nucleus only on average. Furthermore, if formation of these critical size oligomers is rapid compared with their random dimerization, which appears to be the case (Potschka and Schuster, unpublished results), the entire process can be considered as a preequilibrium of oligomers followed by a rate-limiting dimerization step. Then the concentration dependence of nucleation simply relates to the critical oligomer size. Thus, combining the size of the predominant oligomer species, a trimer, with the measured kinetic order of nucleation, $n = 3.5$ (± 0.5) (Figure 5 insert), we calculate an average of 11 subunits for the size of the critical reaction intermediate. A slightly smaller value for the kinetic order of nucleation, $n = 3.0$, has been reported by Adiarte et al. (1975). The formation of overshoot size polymers during this first phase may result in an overestimate of the kinetic order of nucleation. For larger polymers and fast nucleation rates, the elongation reaction would become rate limiting [cf. Johnson and Borisy (1977)]. Therefore, our first conclusion is that the minimum nucleus size is around 22 subunits but it might be as small as 17 subunits.

(*2*) *Variability of Nucleus Size.* Information about the stability of the nucleus is obtained by comparing rates of subunit dissociation with those of nucleus dissolution. Both rates are expected to vary with temperature and pH, and the overall rate of subunit stripping will also depend on the number of subunits to be consecutively removed and therefore depend on the preperturbation state. Over the limited temperature range studied (Figure 7 insert), the rate of subunit stripping is $k_{off} = 3 \times 10^{-2}$ s^{-1}, the anticipated order of magnitude obtained from temperature jump relaxation measurements (Potschka and Schuster, unpublished results). However, the rate of nucleus dissolution changes dramatically with solution conditions which implies that the nucleus size changes with conditions.

(*3*) *Smallest Polymer Is a Single-Layered Helix.* By selecting conditions where polymers are as unstable as possible, we hoped to trap a polymer as close in size to the minimal nucleus as is achievable. The observed SAXS pattern of this nucleus has two remarkable features: The radius of gyration of the cross section is almost as large as that of helix I polymers found at pH 7, 20 °C, at equilibrium, which demonstrates that the nucleus has the full diameter of TMV helices. The scattering intensity in the one-dimensional Guinier regime is almost identical with oligomers. Given the diameter and the degree of polymerization, the nucleus must be oblate, and it is justified to calculate a thickness, which we find to be a structure which matches that of a single layer of subunits. Thus, our third conclusion is that polymerization of TMVP may proceed in the simplest manner one might envisage, namely, via an intermediate that is a single layer of subunits, such as the one we have observed during depolymerization experiments.

This result, which is at variance with previously proposed models for the assembly of TMVP, depends on two experimental aspects of this study: (1) the kinetic analysis that revealed that polymers of minimal size only exist in measurable quantities under conditions where nucleation and elongation rates are about equal and (2) the availability of high-intensity synchrotron X-rays that permitted structural analysis during the few seconds when these minimal sized polymers can be trapped in sufficient quantity to be detected.

Oligomers. Our static SAXS data of A protein match in all details those of Anderer et al. (1964) obtained in 0.01 N NaOH. Not recognizing the paucidispersity and native as-

sembly state of their samples, those authors erroneously proposed a 16-nm length model.

The topological arrangement of subunits in these oligomers has not even been determined for the trimer. The currently accepted model of a cyclic trimer where one subunit is on top of the other two (Caspar, 1963) was viewed as related to the presumed bilayer disk nature of the principal nucleus which is now known to be incorrect. Judging by the structure of the observed nucleus, trimers are likely to be linear; i.e., all subunits are in lateral contact only. However, due to the presence of monomers and large oligomers, our data do not allow us to definitively decide on the structure of the trimer, nor is it obvious why a linear trimer might be a thermodynamically preferred species at equilibrium.

The observed paucidispersity is, however, in agreement with established facts: The oligomeric A protein, also called 4S protein, predominantly contains trimers (Sarkar, 1960; Caspar, 1963) but actually is a mixture of all sizes of oligomers smaller than the nucleus (Potschka and Schuster, unpublished results) with a number-average degree of polymerization of three subunits (Banerjee & Lauffer, 1966) and a weight-average degree of polymerization of five subunits (Schramm & Zillig, 1955) that increases with increasing concentration (Kazel, 1981). Some 0.1 mg/mL monomers are always present (Ansevin & Lauffer, 1959; Kazel, 1981). Formation of larger size oligomers is manifested kinetically and by an increase to 5–6 S (Potschka and Schuster, unpublished results), and even 8–12 S at alkaline pH (Potschka, 1983). Evidence about size and structure of these larger intermediates has been incomplete (Kazel, 1981; Schramm & Zillig, 1955; Caspar, 1963; Vogel et al., 1979; Butler & Durham, 1977). Our data indicate that the larger oligomers and the nucleus interconvert rapidly at low temperature or high pH. Thus, it is not straightforward to interpret sedimentation data, and we defer this discussion to a forthcoming publication.

Kinetics of Nucleation. In the present and previous reports (Scheele & Schuster, 1975; Schuster et al., 1979; Potschka, 1983; Potschka and Schuster, unpublished results), we have demonstrated that polymerization of TMVP proceeds via a nucleation-controlled mechanism in a single pathway resulting in overshoot formation. Thus far, this transient size overshoot has been monitored by turbidity, light scattering, electron microscopy, radius of gyration of cross section, sedimentation values, proton uptake, and temperature jump relaxation kinetic methods. Aided by the present results from time-resolved X-ray solution scattering measurements, we are now able to present a detailed picture of the kinetic events during formation of polymers.

First, large oligomers that are rapidly formed from small oligomers (~4 S) combine slowly to form single-layered structures which are the minimum nucleus size. These nuclei then elongate rapidly by addition of small oligomers before the nuclei have reached their equilibrium number. Because the number of slow-forming nuclei is transiently lower than the true equilibrium number of polymers for that set of conditions, the ensuing elongation polymerization occurs to an extent greater than that at true equilibrium, and there is a transient overshoot in the average degree of polymerization. At the point of maximum size overshoot, the rate of polymerization slows sharply into the next slower phase. The sharpness of the transition between the first and second phases is related to the extent of overshoot formed. During the second phase, nuclei continue to be formed, but the concentration of oligomers is low at this stage, and both the overall rate of nucleus formation and the rate of elongation decrease sharply. During this second phase, the average size of the existing polymer distribution decreases. As the concentration of oligomers decreases too, the rate of polymer formation gradually approaches the third phase of final approach to equilibrium (Schuster et al., 1980). However, during the second phase, yet another process is superimposed, namely, the rearrangement of the particle size distribution from the initial kinetically determined very narrow Poisson distribution to the final broader equilibrium distribution of helical rods (Potschka & Schuster, 1987). If this equilibrium process contributes sufficiently to the observable parameter (such as turbidity), another break in rates may be observed between the second and the third phases.

Both the extent and time of equilibration of overshoot polymerization are very dependent on pH, temperature, and protein concentration. Generally, the rate of overshoot polymer formation is much faster than the subsequent approach to equilibrium. Although not shown in the present report, we have carried out SAXS temperature cycling experiments. Similar cycling experiments were performed previously using turbidity measurements to monitor TMVP assembly–disassembly reactions (Schuster et al., 1979). The SAXS results are in qualitative agreement with the previous results and reveal conservation of nuclei during the brief low-temperature cycle.

Polymorphism and Viral Assembly. Our data provide evidence for new and more detailed mechanistic aspects of TMVP assembly at 100 mM ionic strength and corroborate the notion of a unified mode of nucleation. We have characterized single-layered intermediates which are proposed to be central in the polymerization process for which a helical packing of subunits is the most likely one. However, different TMVP structures do exist in solutions at high ionic strength (Raghavendra et al., 1985a) where TMVP forms crystals and different kinds of stacked disks. It is noteworthy that a protein subunit can pack in three different arrangements, depending on reaction conditions. That is, high ionic strength induces stacks of cylindrical bilayer disks whereas temperature-induced polymerization at 100 mM ionic strength produces either $16^1/_3$ or $17^1/_3$ subunit per turn helices. We have presented evidence that the formation of both helical polymorphs is nucleated by the corresponding single-turn structure. Preliminary spectroscopic measurements indicate a structural similarity between high ionic strength stacked disk aggregates and the pH 8 low ionic strength 8S protein (M. Potschka and K. Raghavendra, unpublished results). One can speculate that a single-layer disk may be the nucleation species for the formation of both the limited and extended stacked disk structures observed by electron microscopy, sedimentation, and X-ray diffraction (Durham, 1972; Bloomer et al., 1978; Raghavendra et al., 1985a, 1986, 1988). The fact that subunit packing polymorphism is seen in the assembly of other virus proteins, tubulin and hemoglobin S, suggests that a more detailed understanding of this phenomenon will contribute to an elucidation of general rules for protein–protein interactions. Clearly, further investigations will be required to resolve the mechanism of TMV reconstitution from the coat protein and homologous RNA.

References

Adiarte, A. L., Vogel, D., & Jaenicke, R. (1975) *Biochem. Biophys. Res. Commun. 63*, 432–440.

Anderer, F. A., Kratky, O., & Lo, R. (1964) *Z. Naturforsch., B: Anorg. Chem., Org. Chem., Biochem., Biophys., Biol. 19B*, 906–916.

Ansevin, A. T., & Lauffer, M. A. (1959) *Nature (London) 183*, 1601–1602.
Banerjee, K., & Laufer, M. A. (1966) *Biochemistry 5*, 1957–1964.
Bernal, J. D., & Fankuchen, I. (1941) *J. Gen. Physiol. 28*, 111–146.
Bloomer, A. C., & Butler, P. J. G. (1986) in *The Plant Viruses* (Van Regenmortel, M. H. V., & Fraenkel-Conrat, H., Eds.) pp 19–57, Plenum, New York.
Bloomer, A. C., Champness, J. N., Bricogne, G., Staden, R., & Klug, A. (1978) *Nature (London) 276*, 362–368.
Bordas, J., Koch, M. H. J., Clout, P. N., Dorrington, E., Boulin, C., & Gabriel, A. (1980) *J. Phys. E 13*, 938–944.
Bordas, J., Mandelkow, E. M., & Mandelkow, E. (1983) *J. Mol. Biol. 164*, 89–135.
Butler, P. J. G. (1984) *J. Gen. Virol. 65*, 253–279.
Butler, P. J. G., & Klug, A. (1971) *Nature (London), New Biol. 229*, 47–50.
Butler, P. J. G., & Durham, A. C. H. (1977) *Adv. Protein Chem. 31*, 187–251.
Caspar, D. L. D. (1956) *Nature (London) 177*, 928–929.
Caspar, D. L. D. (1963) *Adv. Protein Chem. 18*, 37–121.
Caspar, D. L. D. (1976) in *Structure–Function Relationships of Proteins* (Markham, R., & Horne, R. W., Eds.) pp 85–99, Elsevier/North-Holland, New York.
Correia, J. J., Shire, S., Yphantis, D. A., & Schuster, T. M. (1985) *Biochemistry 24*, 3292–3297.
Durham, A. C. H. (1972) *J. Mol. Biol. 67*, 289–305.
Durham, A. C. H., & Finch, J. T. (1972) *J. Mol. Biol. 67*, 307–314.
Durham, A. C. H., & Klug, A. (1972) *J. Mol. Biol. 67*, 315–332.
Esau, K. (1968) *Viruses in Plant Hosts*, University of Wisconsin Press, Madison, WI.
Fedorov, B. A. (1971) *Acta Crystallogr., Sect. A: Cryst. Phys., Diffr., Theor. Gen. Crystallogr. A27*, 35–42.
Franklin, R. E. (1956) *Nature (London) 177*, 929–930.
Gabriel, A. (1977) *Rev. Sci. Instrum. 48*, 1303–1305.
Guinier, A., & Fournet, G. (1955) in *Small-Angle Scattering of X-rays*, Wiley, New York.
Hendrix, J., Koch, M. H. J., & Bordas, J. (1979) *J. Appl. Crystallogr. 12*, 467–472.
Hirth, L., & Richards, K. E. (1981) *Adv. Virus Res. 26*, 145–199.
Holmes, K. C., Stubbs, G. J., Mandelkow, E., & Gallwitz, E. (1975) *Nature (London) 254*, 192–196.
Jardetzky, O., Akasaka, K., Vogel, D., Morris, S., & Holmes, K. C. (1978) *Nature (London) 273*, 564–566.
Johnson, V. A., & Borisy, G. G. (1977) *J. Mol. Biol. 117*, 1–31.
Kazel, L. (1981) Ph.D. Thesis, Johns Hopkins University, Baltimore, MD.
Klug, A. (1983) *Biosci. Rep. 3*, 395–430.
Klug, A., & Durham, A. C. H. (1972) *Cold Spring Harbor Symp. Quant. Biol. 36*, 449–460.
Koch, M. H. J., & Brendall, P. (1981) in *Proceedings of the Digital Equipment Computer User Society*, pp 13–16, Warwick, UK.
Koch, M. H. J., & Bordas, J. (1983) *Nucl. Instrum. Methods Phys. Res. 208*, 461–469.
Kratky, O. (1982) in *Small Angle X-ray Scattering* (Glatter, O., & Kratky, O., Eds.) pp 361–386, Academic, London.
Kratky, O., Paletta, B., Porod, G., & Strohmaier, K. (1957) *Z. Naturforsch., B: Anorg. Chem., Org. Chem., Biochem., Biophys., Biol. 12B*, 287–292.
Lauffer, M. A. (1975) *Entropy Driven Processes in Biology*, Springer, New York.
Lauffer, M. A., Shalaby, R. A., & Khalil, M. T. (1967) *Chimia 21*, 460–462.
Mandelkow, E., Holmes, K. C., & Gallwitz, U. (1976) *J. Mol. Biol. 102*, 265–285.
Mandelkow, E., Stubbs, G., & Warren, S. (1981) *J. Mol. Biol. 152*, 375–386.
Meek, K. M., Elliot, G. F., Sayers, Z., Whitburn, S. B., & Koch, M. H. J. (1981) *J. Mol. Biol. 149*, 477–488.
Mittelbach, P. (1964) *Acta Phys. Austriaca 19*, 53–102.
Namba, K., & Stubbs, G. (1986) *Science (Washington, D.C.) 231*, 1401–1406.
Okada, Y. (1986) *Adv. Biophys. 22*, 95–145.
Paglini, S., & Lauffer, M. A. (1968) *Biochemistry 7*, 1827–1835.
Porod, G. (1982) in *Small Angle X-ray Scattering* (Glatter, O., & Kratky, O., Eds.) pp 17–51, Academic, London.
Potschka, M. (1981) *Biophys. J. 33*, 260a.
Potschka, M. (1983) Dissertation Universitaet Wien, Austria.
Potschka, M., & Schuster, T. M. (1987) *Anal. Biochem. 16*, 70–79.
Raghavendra, K., Adams, M. L., & Schuster, T. M. (1985a) *Biochemistry 24*, 3298–3304.
Raghavendra, K., Adams, M. L., & Schuster, T. M. (1985b) *Biophys. J. 47*, 51a.
Raghavendra, K., Salunke, D. M., Caspar, D. L. D., & Schuster, T. M. (1986) *Biochemistry 25*, 6276–6279.
Raghavendra, K., Kelly, J. A., & Schuster, T. M. (1988a) *Biophys. J. 53*, 114a.
Raghavendra, K., Kelly, J. A., Khairallah, L., & Schuster, T. M. (1988b) *Biochemistry 27*, 7583–7588.
Renner, W., Mandelkow, E. M., Mandelkow, E., & Bordas, J. (1983) *Nucl. Instrum. Methods Phys. Res. 208*, 535–540.
Sarkar, S. (1960) *Z. Naturforsch., B: Anorg. Chem., Org. Chem., Biochem., Biophys., Biol. 15B*, 778–786.
Scheele, R. B., & Lauffer, M. A. (1967) *Biochemistry 6*, 3076–3081.
Scheele, R. B., & Schuster, T. M. (1974) *Biopolymers 13*, 275–288.
Scheele, R. B., & Schuster, T. M. (1975) *J. Mol. Biol. 94*, 519–525.
Schramm, G., & Zillig, W. (1955) *Z. Naturforsch., B: Anorg. Chem., Org. Chem., Biochem., Biophys., Biol. 10B*, 493–499.
Schuster, T. M., Scheele, R. B., & Khairallah, L. H. (1979) *J. Mol. Biol. 127*, 461–485.
Schuster, T. M., Scheele, R. B., Adams, M. L., Shire, S. J., Steckert, J. J., & Potschka, M. (1980) *Biophys. J. 32*, 313–329.
Shire, S. J., Steckert, J. J., & Schuster, T. M. (1979) *J. Mol. Biol. 127*, 487–506.
Shire, S. J., Steckert, J. J., & Schuster, T. M. (1981) *Proc. Natl. Acad. Sci. U.S.A. 78*, 256–260.
Spann, U., Renner, W., Mandelkow, E. M., Bordas, J., & Mandelkow, E. (1987) *Biochemistry 26*, 1123–1132.
Steckert, J. J. (1982) Ph.D. Thesis, University of Connecticut, Storrs, CT.
Steere, R. L. (1963) *Science (Washington, D.C.) 140*, 1089–1090.
Stubbs, G. (1984) in *Biological Macromolecules and Assemblies* (Juranek, F. A., & McPherson, A., Eds.) Vol. 1, Wiley, New York.

Stubbs, G., Warren, S., & Holmes, K. (1977) *Nature (London) 267*, 216–221.
Turner, D. R., Mondragon, A., Fairall, L., Bloomer, A. C., Finch, J. T., VanBoom, J. H., & Butler, P. J. G. (1986) *Eur. J. Biochem. 157*, 269–274.
Vogel, D., DeMarcillac, G. D., Hirth, L., Gregori, E., & Jaenicke, R. (1979) *Z. Naturforsch., C: Biosci. 34C*, 782–792.

Solution Structure of Apamin Determined by Nuclear Magnetic Resonance and Distance Geometry†

Joseph H. B. Pease and David E. Wemmer*
Department of Chemistry and Chemical Biodynamics Division, Lawrence Berkeley Laboratory, University of California, Berkeley, California 94720
Received May 9, 1988; Revised Manuscript Received July 1, 1988

ABSTRACT: The solution structure of the bee venom neurotoxin apamin has been determined with a distance geometry program using distance constraints derived from NMR. Twenty embedded structures were generated and refined by using the program DSPACE. After error minimization using both conjugate gradient and dynamics algorithms, six structures had very low residual error. Comparisons of these show that the backbone of the peptide is quite well-defined with the largest rms difference between backbone atoms in these structures of 1.34 Å. The side chains have far fewer constraints and show greater variability in their positions. The structure derived here is generally consistent with the qualitative model previously described, with most differences occurring in the loop between the β-turn (residues 2–5) and the C-terminal α-helix (residues 9–17). Comparisons are made with previously derived models from NMR data and other methods.

Apamin is a small neurotoxic peptide component of honey bee venom. Like many other peptide neurotoxins, apamin has a high cystine content and a high basicity, but apamin is different from most peptide toxins in its unusual ability to cross the blood brain barrier and act on the central nervous system (Habermann, 1972). Apamin is known to block calcium-dependent potassium fluxes, possibly by binding to a Ca^{2+}-dependent potassium channel (Banks et al., 1974). Additionally, apamin serves as a model for understanding various aspects of peptide folding and amide proton exchange. To determine the structural basis of its activity and for interpretation of other experimental results, it is important to have a good understanding of the structure of this peptide. Apamin contains 18 amino acids with two disulfides (see Figure 1), which give it an extremely stable structure with respect to temperature, pH, and denaturants, not unfolding completely even at 70 °C in 6 M guanidinium hydrochloride (Miroshnikov et al., 1978; N. V. Kumar, personal communication). During the past few years there have been a number of studies aimed at determination of apamin's structure, using energy refinements (Freeman et al., 1986; Hider & Ragnarsson, 1981), circular dichroism (CD)[1] (Miroshnikov et al., 1978), and nuclear magnetic resonance spectroscopy (NMR) (Wemmer & Kallenbach, 1983; Okhanov et al., 1980; Bystrov et al., 1978). Here we use two-dimensional proton NMR data with distance geometry to obtain an improved picture of apamin's solution structure.

Previously, two-dimensional NMR was used to obtain almost complete assignments of apamin's proton NMR spectrum (Wemmer & Kallenbach, 1983).[2] As with many other peptides, the sequential assignment pattern and identification of slowly exchanging amides gave information about the secondary structure of the molecule. Using this information, Wemmer and Kallenbach (1983) derived a model that was consistent with the previously reported CD data (Miroshnikov et al., 1978) and ϕ angles from $^3J_{NH-\alpha H}$ coupling constants (Bystrov et al., 1980). Hider et al. (1986) have also developed structural models for apamin based on energy refinement methods, and Bugg and co-workers[3] have used coordinates from their crystal structure of a scorpion toxin, for which one section seemed to be structurally similar to apamin, together with modeling and energy refinement to develop a structural model. In this work we describe the detailed structure obtained from further NMR measurements and our distance geometry calculations and compare the previously derived structural models with it.

Materials and Methods

NMR Spectroscopy. All two-dimensional nuclear Overhauser effect (NOESY) spectra (Anil-Kumar et al., 1980; Jeener et al., 1979) were recorded on a 500-MHz General

† Supported by the Office of Energy Research, Office of Health and Environmental Research, Health Effects Research Division of the U.S. Department of Energy under Contract DE AC03-76SF00098 and through instrumentation grants from the U.S. Department of Energy, DE FG05-86ER75281, and the National Science Foundation, DMB 86-09035.

[1] Abbreviations: NMR, nuclear magnetic resonance; NOESY, nuclear Overhauser effect spectroscopy; TPPI, time proportional phase incrementation; NOE, nuclear Overhauser effect; CD, circular dichroism; standard single-letter abbreviations for amino acids (A = alanine, C = cysteine, E = glutamic acid, H = histidine, K = lysine, L = leucine, N = asparagine, P = proline, Q = glutamine, R = arginine, T = threonine).

[2] Some of the previously reported assignments are corrected in the present work. These are the Cys 1 β-protons (3.12 and 2.74 ppm), the Pro 6 α-proton (4.66 ppm), the Pro 6 β-protons (1.90 and 1.75 ppm), and the Glu 7 β-protons (2.25 and 2.08 ppm). Chemical shifts are indirectly referenced to TSP through assignment of $\delta(H_2O)$ = 4.75 ppm at 30 °C.

[3] C. E. Bugg, A. Zell, M. Carson, M. Epps, and J. Hermans, personal communication.

0006-2960/88/0427-8491$01.50/0